Published in final edited form as:
J Comp Neurol. 2012 June 1; 520(8): 1737–1750. doi:10.1002/cne.23010.

Failure of lower motor neuron radial outgrowth precedes retrograde degeneration in a feline model of SMA

Erin N. Wakeling[1,*], **Béatrice Joussemet**[2,*], **Patrick Costiou**[3], **Dominique Fanuel**[3], **Philippe Moullier**[2,4,5], **Martine Barkats**[6], and **John C. Fyfe**[7]

[1] Genetics Program, Michigan State University East Lansing, MI, USA

[2] Laboratoire de Thérapie Génique, INSERM UMR649, Nantes, France

[3] National Veterinary School of Nantes, ONIRIS, Nantes, France

[4] Department of Molecular Genetics & Microbiology, University of Florida, Gainesville, FL, USA

[5] GENETHON, 91000 Evry, France

[6] UMR974 INSERM-UPMC-CNRS-AIM Institut de Myologie, Paris, France

[7] Department of Microbiology & Molecular Genetics, Michigan State University, East Lansing, MI, USA

Abstract

Feline SMA is a fully penetrant, autosomal recessive lower motor neuron disease in domestic cats that clinically resembles human SMA Type III. A whole genome linkage scan identified a ~140 kilobase deletion that abrogates expression of *LIX1*, a novel SMA candidate gene of unknown function. To characterize the progression of feline SMA, we assessed pathological changes in muscle and spinal cord from 3 days of age to beyond onset of clinical signs. EMG analysis indicating denervation occurred between 10 and 12 weeks, with the first neurological signs occurring at the same time. CMAP amplitudes were significantly reduced in the soleus and extensor carpi radialis muscles at 8 to 11 weeks. Quadriceps femoris muscle fibers from affected cats appeared smaller at 10 weeks; by 12 weeks atrophic fibers were more prevalent than in age-matched controls. In affected cats, significant loss of L5 ventral root axons was observed at 12 weeks. By 21 weeks of age, affected cats had 40% fewer L5 motor axons than normal. There was no significant difference in total L5 soma number, even at 21 weeks; thus degeneration begins distal to the cell body and proceeds retrogradely. Morphometric analysis of L5 ventral roots and horns revealed that 4 weeks prior to axon loss, motor axons in affected cats failed to undergo radial enlargement, suggesting a role for the putative disease gene, LIX1, in radial growth of axons.

Keywords

spinal muscular atrophy; motor neuron; neurodegeneration

Corresponding author: Erin N. Wakeling B307 Life Sciences Building Michigan State University East Lansing, MI 48824 (517) 355-6477 wakelin1@msu.edu.

*These authors contributed equally to this work.

Introduction

The human spinal muscular atrophies (SMA) are a group of lower motor neuron disorders that vary in age of onset, clinical severity and survival time. Individuals with the severest form (SMA I; Werdnig-Hoffmannn disease) never gain the ability to sit upright or walk and do not survive beyond a few years of age. Type II SMA patients develop clinical symptoms after six months of age and are unable to walk. SMA III (Kugelberg-Welander disease) is the mildest juvenile onset form of the disease; individuals are able to walk, although this ability may be lost as the disease progresses. The adult-onset form of the disease (SMA IV) has the mildest clinical severity and does not result in shortened life expectancy (Russman, 2007). SMA is the leading genetic cause of infant mortality, and mutations in the ubiquitously expressed *survival of motor neuron 1* (*SMN1*) account for 98% of cases (Lefebvre et al., 1995; Wirth et al., 1999). Copy number variation in a nearly identical gene, *survival of motor neuron 2* (*SMN2*), modifies clinical severity; eight copies are sufficient to complement homozygous loss of *SMN1* (Wirth et al., 2006). Only 10% of *SMN2* transcripts are full-length due to a single nucleotide difference in exon 7 that disrupts an exonic splice enhancer (Lorson et al., 1999; Lorson and Androphy, 2000; Monani et al., 1999). Currently, there is limited understanding of the mechanisms by which mutations of ubiquitously expressed genes result in SMA and other motor neuron specific diseases, such as amyotrophic lateral sclerosis (ALS) and spinal bulbar muscular atrophy (SBMA). Approaches to SMA treatment have focused on pharmacologically increasing levels of full length SMN produced from the *SMN2* locus or *SMN1* gene therapy (Burnett et al., 2009). Naturally occurring and engineered animal models offer insight into motor neuron development and maintenance that is critical for the discovery and testing of effective treatments.

Feline SMA is a fully penetrant, autosomal recessive disease resembling SMA III in severity and time of onset (He et al., 2005). In affected cats, lower motor neuron degeneration leads to muscle atrophy and gait abnormalities. Affected cats demonstrate clinical signs at 12 to 13 weeks of age with disease progression reaching a plateau around 8 months. Life expectancy is ~8 years. A whole genome linkage scan and fine mapping identified a 140 kilobase deletion that disrupts expression of *limb expression 1* (*LIX1*) and *leucyl/cystinyl aminopeptidase (LNPEP*) (Fyfe et al., 2006). We hypothesize that *LIX1* is the feline SMA disease gene because it is highly expressed in the spinal cord and a *LNPEP* knockout did not produce an overt neuromuscular phenotype (Moeller et al., 2002; Keller et al., 2002). LIX1 is poorly annotated but is predicted to possess a double-stranded RNA binding domain at its amino terminus (Giot et al., 2003; Fyfe et al., 2006). This is particularly intriguing because SMN is critical for small nuclear ribonucleic protein (snRNP) biogenesis (Pellizzoni et al., 1998, 2002; Massenet et al., 2002) and co-localizes with mRNA granules in motor neurons (Zhang et al., 2007). Thus far only the end-stage of feline SMA pathology has been reported. In this study we sought to characterize the onset and progression of disease through histological and morphometric techniques.

Materials and Methods

Animals

Cats in this study were members of an out-crossed family derived from a purebred Maine coon cat and a domestic short hair (Fyfe et al., 2006). All cats were produced and housed in breeding colonies at Michigan State University (MSU) or at the Nantes Veterinary School (Centre de Boisbone, ONIRIS, Nantes, France). Animals at MSU were raised and euthanized according to protocols approved by the university's Institutional Animal Care and Use Committee (IACUC) and which adhered to National Institutes of Health guidelines. Experiments performed at the Nantes Veterinary School were approved by the regional

ethics committee and were carried out according to European guidelines for the care and use of experimental animals. Cats were genotyped by multiplex PCR as previously described (Fyfe et al., 2006).

Neurological examinations and electromyography

The SMA signs, previously described (He et al., 2005), were followed in four affected kittens and compared with three unaffected heterozygous littermates, from the age of 4 to 36 weeks, by neurological examinations and electromyography (EMG) tests. Neurological tests were developed by veterinary neurologists at the Nantes Veterinary School based on a commonly used neurological examination protocol (De Lahunta, 2001). Different parameters relative to the behavior of the animal, the muscular strength, the postural reactions and reflexes were scored according to severity as follows: 0, normal; 1, moderately abnormal; 2, clearly abnormal; 3, severely abnormal (see Supplementary Table 1 for detailed neurological exam rubric). During the behavioral tests, we encouraged the kitten to play and scored the position of the limbs (a lateral deviation of the limbs with an increased base-width of the support polygon were usually observed in SMA kittens, Figure 1), the presence of muscle tremors, the breathing frequency, the sway of the hindquarter and the time in a seated position compared with normal kittens. Other parameters, such as the muscle tone developed in reaction to an extension of the hind-limbs, the size of the anterior tibialis muscle compared with normal kittens of the same age, the proprioceptive reactions of all limbs (delayed in SMA cats) and some postural reactions including the ability to coordinate movement and walk using two limbs (hemi-locomotion) were also scored as described above. All the scores obtained during the neurological exam, conducted by a veterinary neurologist who was blind to the cat's genotype, were added to obtain a global score (0 to 24) per animal.

EMGs were conducted every 2 or 3 weeks in the same animals with a Neuropack 2 EMG apparatus (Nihon Kohden, Nishiochiai, Japan) according to usual procedures previously described in cats and dogs (Cuddon, 2002). The biceps femoris, sartorius, tibialis anterior, gastrocnemius and plantaris muscles of the two hindlimbs were tested. For each muscle, a global score accounting for the presence and the frequency of fibrillation potentials (0, absence; 1, presence in some regions; 2, presence in multiple regions; 3, presence in all regions tested), abnormal insertion potentials (0, absence; 1, presence) and high-frequency discharges (0, absence; 1, presence) was assigned. Additionally, compound motor action potential (CMAP) amplitudes and nerve conduction velocities (NCV) were measured in the soleus muscle after stimulation of the sciatic nerve or in the extensor carpi radialis muscle after stimulation of the radial nerve.

Histology

Quadriceps femoris muscles from two affected cats and two age matched controls (homozygous normal and heterozygous) at 6, 8, 10, 12 and 21 weeks were fixed by immersion in 10% neutral buffered formalin, paraffin embedded, sectioned and stained with hematoxylin-eosin (H&E). Unfixed tibialis anterior (TA), extensor digitorum longus (EDL) and soleus muscles from 10 and 12 week old cats were embedded in Tissue-Tek® OCT medium (Sakura Finetek, Torrance, CA) and frozen in liquid nitrogen cooled 95% ethanol. Muscles were stored at -80°C until transversely sectioned at 12 μm with a cryostat and thaw mounted on gelatin-coated glass slides. Muscle sections were fiber-typed by ATPase enzymatic reactions at pH 4.6 and 9.4. Five random, non-overlapping images taken with a 40× objective of a single H&E section and 2 images acquired with a 10× objective of a fiber-typed section per cat were captured on an Eclipse 90i microscope with a DS-Fi1 digital camera (Nikon, Tokyo, Japan) for fiber shape examination. The diameters of 50 adjacent fibers in H&E stained quadriceps femoris muscle sections from 6, 8-9 and 10 week old cats

were measured with NIS Elements software (Nikon, Tokyo, Japan) in a single image acquired with a 40× objective.

One fifth of the frozen sections were screened for neuromuscular junctions (NMJs) with a modified cholinesterase stain (Pestronk and Drachman, 1978). Prior to enzymatic staining, sections were warmed to room temperature and fixed in 4% paraformaldehyde in 0.1 M sodium phosphate buffer pH 7.4. Staining was terminated after 15 minutes with distilled water; sections were dehydrated with graded ethanol washes, cleared with xylene and cover-slipped with Permount (Thermo Fisher Scientific, Waltham, MA). Sections were examined for the presence of motor endplates. Sections adjacent to those exhibiting cholinesterase staining were labeled for acetylcholine receptors by sequential incubation in 1:500 dilution of biotin conjugated α-bungarotoxin (Invitrogen, Carlsbad, CA), avidin horseradish peroxidase conjugate (Kirkegaard and Perry Laboratories, Gaithersburg, MD) and NovaRed™ peroxidase substrate (Vector Laboratories, Burlingame, CA).

Tissue-Tek® OCT embedded TA and EDL muscles were also longitudinally sectioned at 20 μm with a cryostat and thaw mounted on gelatin-coated glass slides. To label the pre and post-synaptic regions of the NMJs, sections were first stained for acetylcholine receptors as above, except that the peroxidase substrate was Vector® Red (Vector Laboratories, Burlingame, CA). Sections were then labeled with a 1:1000 dilution of mouse anti-phosphorylated neurofilaments antibody cocktail SMI312; Abcam, Cambridge, MA) and a 1:500 dilution of Alexa Fluor® 488 labeled goat anti-mouse IgG (Invitrogen, Carlsbad, CA). Sections were cover-slipped in ProLong Gold antifade reagent (Invitrogen, Carlsbad, CA) and stored at 4°C in the dark for laser scanning confocal microscopy.

Spinal cords were fixed by immersion in 10% neutral buffered formalin and the L5 ventral roots and L5 segment were dissected. L5 spinal cord segments were paraffin embedded and thirty-two 10 μm thick serial sections were stained with cresyl violet for cell body counts and morphometric analysis. L5 ventral roots were embedded in Poly/Bed 812- Araldite, thick sectioned and stained with toulidine blue for axon counts and morphometry.

Antibody characterization

The SMI-312 antibody (Table 1) used is a pan-neurofilament (NF) marker that detects phophorylated NFs in axons of fetal and newborn humans (Sternberger and Sternberger, 1983; Ulfig et al., 1998; Haynes et al., 2005). It is a cocktail of mouse monoclonal antibodies against heavily phosphorylated epitopes on NF-M and NF-H. On western blots of cat spinal cord lysate, SMI-312 detected 200 and 160 kDa bands. Staining was eliminated by incubation of the membranes in calf intestine alkaline phosphatase (New England Biolabs, Ipswich, MA) prior to the blocking step.

Motor neuron and myelin sheath morphometry

All axons within a single, toulidine blue stained cross-section of L5 ventral roots were counted with Neurolucida (MBF Bioscience, Williston, VT) and a Nikon FX-A microscope (Tokyo, Japan) equipped with a 20x objective. Non-overlapping images of ventral root cross sections were captured with a 40× objective. Diameters of two hundred and fifty axons, excluding the myelin sheath, were measured from these images with Image-Pro Plus 5.1 (Media Cybernetics, Bethesda, MD). To prevent sampling bias, measurements began in the upper left hand corner of the image and then proceeded axon by axon horizontally and then vertically through the image until 250 axons were measured. Axon diameters were grouped in 2 μm increments, and the percent of axons within each bin was determined.

Average myelin sheath thicknesses were also determined from the toluidine blue stained ventral root images. Using Image-Pro Plus 5.1, two concentric circles were fitted to one

hundred axons. The larger circle contained the axon and myelin sheath; and the smaller circle contained only the axon. Subtraction of the smaller radius from the larger radius was taken as the myelin sheath thickness.

All cresyl violet positive motor soma with a distinct nucleus and nucleolus at 10× magnification were counted with Neurolucida in 16 alternate, 10 μm thick cross-sections of L5 spinal cord. Raw counts were corrected for over-counting with Abercrombie's formula, P = A(M/M+L) , where P is the corrected count, A is the raw count, M is section thickness and L is the nucleolar diameter (Abercrombie, 1946). Only a single ventral horn was counted in each section. Non-overlapping images of a single cross section were collected with a 10× objective for cell body morphometrics. In five images the major and minor diameters of all motor soma with distinct nucleoli were measured by fitting two circles to the soma, one that was contained within the soma and one that surrounded the soma (Tatton et al., 1988), with Image Pro 5.1. Major and minor diameters were averaged to obtain the average soma diameter. The average diameters were grouped in 10 μm increments and the percent of cell bodies within each bin was determined.

Confocal laser scanning microscopy

Stained longitudinal muscle sections were examined for fluorescence on an Olympus Fluoview 1000 laser-scanning microscope (Center Valley, PA) equipped with a 40× oil immersion objective NA=1.30. Autofluoresence of Vector® Red labeled acetylcholine receptors (magenta) was excited at 542 nm, and emission was detected through a long pass 560 nm filter. Fluorescence of Alexa Fluor 488 labeled neurofilaments (green) was excited at 488 nm, and emission was detected through a band pass 505-525 nm filter. Structural integrity of NMJs was determined in magenta-green merged extended focus images that were optimized for brightness and contrast with Fluoview v5 software. Junctions in which magenta and green signals failed to overlay were scored as denervated.

Data analysis and figure generation

Averages, standard deviations (S.D.), two-tailed Student's t-test (α=0.05), X^2 test and all graphs were generated with Microsoft Excel® (Microsoft Corporation Redmond, WA). Mann Whitney U tests were performed in SigmaStat v3.1 (Aspire Software International, Ashburn, VA). Where numbers or diameters of axons or cell bodies are given, they were determined on only one side of the animal, rather than both sides of the same individual. Figures were created and sized in Microsoft PowerPoint® and then converted to TIFF format in Adobe Photoshop® CS4 (San Jose, CA).

Results

Neurological and EMG examinations were performed at two week intervals between four and 36 weeks of age in four affected (A) and three normal (N) kittens. Before the age of 10 weeks, affected and normal animals showed no statistical differences (Figure 2A, t-test $p>0.05$). At 12 weeks of age, affected cats developed neurological signs ($N=0.5 \pm 0.5$, $A=6.6 \pm 1.7$; t-test $p<0.05$); several fibrillation potentials and high-frequency discharges appeared in the hind limb (Figure 2B) and forelimb muscles (data not shown), suggesting a process of muscle denervation. Moreover, between 8 and 11 weeks, we detected a significant decrease in CMAP amplitudes recorded in the soleus muscle (Figure 2C). NCVs measured in the sciatic and the radial nerves appeared decreased at 16 weeks in the four affected cats compared with three normal kittens (Figure 2D), but the difference did not reach statistical significance.

We examined muscle fiber morphology in quadriceps femoris muscle of two normal and two affected cats aged 6, 8, 10, 12 and 21 weeks (Figure 3). We observed no noticeable difference in fiber shape or size at 6 and 8 weeks of age (Figure 3A-D, Supplementary Table 1). At 10 weeks (Figure 3E and F), affected cats had smaller muscle fiber diameters than age-matched controls (N=17.2 ± 3.8 μm and N=22.9 ± 4.3μ; A=11.6 ± 1.9 μm and 14.5 ± 2.6 μm). Small, angular fibers were more prevalent in affected cats at 12 weeks of age and occasional centralized nuclei were observed. Groups of atrophic fibers and hypertrophied muscle fibers were observed in affected cats at 21 weeks (Figure 3J). Fiber typing of TA and EDL muscles (Figure 4A, B, C, D) at 12 weeks of age (n=2) revealed both slow twitch (Type I) and fast twitch (Type 2) atrophic fibers. However, the majority of atrophic fibers in the TA and EDL were fast twitch. In affected TA muscles, 12.7% and 17.6% of fast twitch fibers were atrophied compared with the 3.3% and 5.6% of slow twitch fibers that were atrophied. In affected EDL muscles, 23.1% and 30% of fast twitch fibers were atrophic, whereas only 3.2% and 5.1% of slow twitch fibers were atrophic. Concordantly, we observed few atrophic fibers in the soleus (Figure 4E and F), a slow twitch muscle, of affected cats. These observations indicated that neurons innervating fast twitch muscle fibers are primarily affected in feline SMA.

Neuromuscular junctions (NMJs) in the TA and EDL muscles of affected cats were structurally intact at 10 weeks of age (Figure 5B and D), as compared to a control animal (Figure 5A and C). We observed end-plate denervation at 12 weeks (Figure 5F and H). In the TA muscle, 6 of 21 and 9 of 33 NMJs (28% mean denervation) were denervated in two affected cats. Six of 18 and 9 of 36 NMJs (29% mean denervation) were denervated in EDL muscles of the same affected cats. In the 12 week control animal, only 1 of 15 and none of 18 NMJs were denervated in TA and EDL muscle sections, respectively (Figure 5E and G). No abnormal accumulations of neurofilament were identified in affected cats at either time-point. Therefore, structural disruption of neuromuscular junctions coincided with the presence of atrophic fibers.

To understand the progression of neurodegeneration in feline SMA, we assessed the total number of axons in toluidine blue stained cross sections of L5 ventral roots from affected cats and age-matched controls (Figure 6). At younger ages (3 days and 4.5 weeks) we did not have enough cats to perform statistical tests, however the total number of L5 ventral root axons was comparable in normal and affected cats (Figure 7A). At 6-7, 8-9 and 10 weeks of age, there was no significant difference in L5 ventral root axon number in normal and affected cats. Loss of L5 motor axons coincided with the onset of clinical signs at 12 weeks (N=4544 ± 396, A=3647 ± 369; n=4, t-test p=0.03), and by 21 weeks of age, affected cats had 40% fewer L5 motor axons than the controls (N=4575 ± 648, A=2734 ± 472; n=5, t-test $p=9\times10^{-4}$). In contrast, L5 dorsal root axons of affected cats were never fewer than in normal cats, even at 39 weeks of age (data not shown).

During axon counts we observed a lack of large caliber motor axons in affected cats beginning at 8 weeks of age (Figure 6D). This finding is consistent with previous morphometric analysis of a C5 ventral root in an affected adult cat (He et al., 2005). To investigate this further, we measured axon diameter in 250 L5 ventral root axons in affected and age-matched cats. At 3 days (Figure 7B) the distribution of axon diameters in affected cats was comparable to normal controls. In both groups axons were less than 6 μm in diameter and the overall distribution of axon calibers was unimodal. At 4.5 weeks the overall axon caliber distribution remained unimodal in both normal and affected cats. However, affected cats had a greater number of axons measuring 2 to 4 μm in diameter. Normal cats had axons with diameters up to 10 μm, but no axons greater than 8 μm were found in affected cats. Beginning at 6 weeks of age, normal cats began to develop the characteristic bimodal distribution of ventral root motor axon diameters, but axons in

affected cats maintained a unimodal distribution (Figure 7D). Affected cats had more 2 to 4 μm diameter axons and fewer 4 to 6 μm diameter axons than age matched controls (2 to 4 μm: N=20±0.6%, A=40±1.8%; 4 to 6 μm: N=42±4.6%, A=26± 4.2%; n=3 Mann Whitney p=0.1). Eight week old affected cats had fewer axons with diameters measuring 6 μm and greater (Figure 7E). However, these differences between normal and affected cats at 6 and 8 weeks failed to reach statistical significance by the Mann-Witney U test due to small sample size (n=3). Small caliber axons (2 to 6 μm) were present in greater numbers in affected cats at 8, 10 and 12 weeks. This disparity was even more pronounced at 12 and 21 weeks of age; axons with calibers equal to or greater than 8 μm are significantly reduced in affected cats (Figure 7F,G). Furthermore, axons greater than 16 μm in diameter were never observed in 21 week old affected cats. Overall, the axon caliber distribution in affected cats was significantly different from normal animals at 6 ((X^2=26.8, df=4, p<0.001), 8 (X^2=130.1, df=4, p<0.001), 12 (X^2=277.4, df=7, p<0.001), and 21 weeks (X^2=1859.2, df=8, p<0.001).

No nerve root myelin abnormalities were observed previously in adult affected cats assessed by teased fiber preparation (He et al., 2005). Here, we observed no overt differences in myelin sheath thickness in affected cats at any age examined (Figure 6). To further assess myelin in feline SMA, we measured myelin thickness and axon caliber in the same 100 axons at 8-9, 10, 12 and 21 weeks (Figure 8). Even though a significant decrease in average axon radius was detected at all ages (Figure 8A, t-test p≤0.02), there was no difference in average myelin thickness (Figure 8B).

To determine whether the neurodegeneration in feline SMA precedes in an anterograde or retrograde direction we counted the number of motor neuron cell bodies present in 16 alternate sections (10 μm thick) stained with cresyl etch violet in normal and affected cats aged 8-9, 12 or 21 weeks (Figure 9A-H, representative micrographs). In the length of L5 cord that we examined there was no significant difference in the number of motor neuron somas even at 21 weeks (Figure 9I). However, the presence of chromatolysis and acentric nuclei in anterior horn cells beginning at 8-9 weeks (Figure 9G and H) provided evidence of somal degeneration that may lead to a significant loss of cell body numbers later in the disease progression. This observation of significant axonal loss (at 12 weeks) prior to cell body loss indicated a mechanism of retrograde degeneration.

Morphometric analysis of L5 ventral horn somas also revealed a dearth of large cell bodies, although this phenomenon occurred at a later age than the deficit in large axon diameters in the ventral roots. At 8-9 weeks, affected cats had similar distributions of cell body diameters as age matched controls (Figure 9J). As normal cats aged the percentage of cells greater than 40 μm in diameter increased from 8.1±2.6% at 8-9 weeks to 14.4±2.9% and 19.0±5.7% at 12 and 21 weeks, respectively (Figure 9K, L). In contrast, the percentage of cells greater than 40 μm in affected cats decreased with age. This failure to increase somal size resulted in a significantly lower percentage of cells with diameters greater than 40 μm in affected cats aged 12 and 21 weeks (N=14.4±2.9%, A=3.9±3.1%; n=4, Mann-Whitney p<0.03 and N=19.0±5.7%, A=4.5±1.4%; n=5, Mann-Whitney p<0.008). Thus at 12 and 21 weeks there is as yet no difference in cell body number but the cell bodies present in affected cats are smaller in diameter.

Discussion

We undertook a systematic examination of muscles, motor neuron axons and cell bodies to identify the earliest pathological changes in feline SMA and to follow their progression. Development proceeds normally in affected cats until ~6 weeks of age. At this age, ventral root axons fail to undergo radial enlargement to transform from a unimodal distribution of axon diameters to a bimodal distribution. Significant decreases in compound motor action

potential (CMAP) amplitudes occur at 8 weeks, indicating functional denervation of neuromuscular junctions although L5 root axon numbers remained unchanged and there was no muscle fiber atrophy. The appearance of muscle atrophy coincided with clinical signs, structural denervation of motor end-plates and a statistically significant loss of L5 ventral root axons at 12 weeks of age. Axon loss progressed with age, as 40% of axons were lost by 21 weeks. Despite the significant reduction in ventral root axons, cell body numbers were unaffected even at 21 weeks. As the defects in neuromuscular synaptic transmission occur prior to axon degeneration and L5 cell body numbers are maintained even at 21 weeks, this indicates a process of retrograde degeneration in feline SMA.

Feline SMA resembles the human disease and SMA mouse models in several aspects. Affect cats demonstrate decreases in CMAP amplitudes beginning at 8 weeks of age. Significant decreases in CMAP amplitudes, indicating motor unit loss, are observed in severe and mild human SMA cases (Kugelberg and Welander, 1956; Buchthal and Olsen, 1970; Emery 1971). Despite a reduction in axon caliber, there was no significant decrease in peripheral nerve conduction velocities in SMA affected cats even at 24 weeks of age. This is likely explained by the contribution of sensory axons, which are unaffected in feline and human SMA, to the overall NCV. NCVs are not typically affected in human SMA, although there have been some reports of reduced NCVS in Type I SMA cases (Hausmanowa-Petrusewicz and Fidzianska, 1974; Moosa and Dubowitz, 1976; Murayama et al., 1991).

Myofibrillar ATPase fiber typing of TA, EDL and soleus muscles from affected cats demonstrated atrophic fibers of both types, but that a majority of atrophic fibers were fast twitch with a corresponding hypertrophy of slow twitch fibers. In human SMA, both fiber types are affected in severe SMA, but fast twitch fibers are predominantly atrophied in Type III SMA. Hypertrophy of slow twitch fibers is also observed in human SMA (Walsh et al., 1987; Munsat and Davies, 1992).

Fast twitch muscle fibers belong to larger motor units and are innervated by larger diameter motor neurons than slow twitch fibers (Sato et al., 1977; Purves et al., 2001). Concordantly, morphometric analysis of L5 ventral root axons demonstrated that motor neurons in affected cats failed to develop a normal bimodal size distribution at 6 weeks. The decrease in large caliber axons was echoed in L5 ventral horn somas at 12 weeks of age. Furthermore, motor neurons exhibiting accentric nuclei and chromatolysis were observed. In all types of human SMA, loss of large motor neurons is the most striking neuropathology. The remaining motor neurons are often chromatolytic with accentric nuclei (Byers and Banker, 1961; Ghatak, 1978; Lippa and Smith, 1988; Crawford and Pardo, 1996; Araki et al., 2003; Kuru et al., 2009). The selective vulnerability of large motor neurons has also been observed in SMA mouse models of varying severity (Ferri et al., 2004; Monani et al., 2003). Similar to SMA affected cats, SMA mouse models also display pathology at the neuromuscular junctions and in motor axons before the cell bodies, supporting a mechanism of retrograde degeneration (Cifuentes-Diaz et al., 2002; Ferri et al., 2004; Murray et al., 2008; Michaud et al., 2010).

Feline SMA is a naturally occurring large animal model of human SMA that replicates the pathology and disease progression seen in human and engineered mouse models. Our study supports a defect of axon radial growth as the earliest observed pathological change in feline SMA. Two critical factors in axon diameter regulation are neurofilaments (NFs) and myelin. NFs are intermediate filaments composed of three polypeptides, NF-L (light), NF-M (medium), NF-H (heavy). They are the most abundant cytoskeleton component in neurons. During development, increases in NF expression occur after synapse formation and are concurrent with myelination and axon radial growth (Lee, 1996). Increases in NF expression and transport are also seen after axon crush or transection (Hoffman et al., 1985, 1987). NF-L is critical for neurofilament assembly and axon radial growth (Sakaguchi et al., 1993). The

carboxyl termini of NF-M and NF-H form the side arms of NFs and are heavily phosphorylated in axons. These negatively charged phosphate groups are hypothesized to increase NF spacing and, therefore, axon caliber. Due to the larger number of KSP repeats in NF-H, it was originally thought that the heavy subunit was more important for axon radial growth. However, knockout of NF-H or deletion of its tail domain failed to disrupt radial growth and resulted only in a mild decrease in motor axon number (Rao et al., 1998, 2002). In contrast, deletion of the NF-M tail domain severely inhibited axon caliber expansion (Rao et al., 2003; Garcia et al., 2003). The NF-M tail domain contains few KSP repeats; whose position and number are not conserved and recent evidence suggests that these residues are not required for axon radial growth (Garcia et al., 2009). Abnormal neurofilament accumulation in motor neuron cell bodies and at motor endplates is a hallmark of human SMA (Lippa and Smith, 1988; Murayama et al., 1991; Kuru et al., 2009). In mouse models, the accumulation of neurofilaments at motor end plates is an early pathogenic change (Cifuentes-Diaz et al., 2002; Michaud et al., 2010). We detected no accumulation of neurofilaments at the motor end plates of 10 and 12 week old affected cats, suggesting that neurofilaments disruption may not be involved in feline SMA pathogenesis.

Another key determinant in axon caliber is myelination. Unmyelinated axons have smaller calibers than myelinated fibers. Furthermore, among myelinated axons, myelin thickness is correlated with axon caliber, and the unmyelinated nodes of Ranvier are smaller in diameter than contiguous myelinated axonal segments. Nodes of Ranvier also have reduced neurofilament spacing and phosphorylation (Hsieh et al., 1994). Schwann cells are currently thought to signal to axons via an unidentified receptor to increase cellular kinase activity and neurofilament phosphorylation (Yin et al., 1998; Dashiell et al., 2002). We have excluded demyelination as an explanation of reduced axon caliber in feline SMA, but more work is required to determine expression and phosphorylation levels of neurofilaments in SMA affected cat axons and whether LIX1, the putative disease gene, has a direct role in this or the signaling between Schwann cells and motor neurons.

To the best of our knowledge this is the most intensive, longitudinal study of disease pathogenesis in a SMA animal model. Despite the different genetic basis for the diseases, feline SMA replicates most of the features of human SMA. Thus the knowledge gained from understading feline SMA pathogenesis may lead to insights in human SMA. Furthermore, this animal model provides a large animal system to the research community to identify the most effective delivery methods of gene therapy vectors to the central nervous system and to test neuro-protective compounds for safety and efficacy in treating SMA and other motor neuron diseases.

Supplementary Material

Refer to Web version on PubMed Central for supplementary material.

Acknowledgments

We would like to thank Amy Porter, Kathy Joseph, Rick Rosebury and Ralph Commons of the Michigan State University Histopathology Laboratory for their assistance with muscle, spinal cord and ventral root histology. We also thank Cynthia Jordan and Jessica Poort for their assistance with the neuromuscular junction immunohistochemistry. Finally we would like to thank Lisa St. Charles and Brian Farber for their assistance with the L5 ventral root axon counts.

This study was supported by grants from SMA-Europe (#13841), Association Française contre les Myopathies (#10740 and 11717), the National Institutes of Child Health and Human Development (#HD39888) and the Michigan State University College of Veterinary Medicine Companion Animal Fund.

Literature cited

Abercrombie M. Estimate of nuclear population from microtome sections. Anat Rec. 1946; 94:239–247. [PubMed: 21015608]

Araki S, Hayashi M, Tamagawa K, Saito M, Kato S, Komori T, Sakakihara Y, Mizutani T, Oda M. Neuropathological analysis in spinal muscular atrophy type II. Acta Neuropathol. 2003; 106:441–448. [PubMed: 12898156]

Buchthal F, Olsen PZ. Electromyography and muscle biopsy in infantile spinal muscular atrophy. Brain. 1970; 93:15–30. [PubMed: 5418399]

Burnett BG, Crawford TO, Sumner CJ. Emerging treatment options for spinal muscular atrophy. Curr Treat Options Neurol. 2009; 11(2):90–101. [PubMed: 19210911]

Byers R, Banker B. Infantile muscular atrophy. Arch Neurol. 1961; 5:140–164. [PubMed: 13689565]

Cifuentes-Diaz C, Nicole S, Velasco ME, Borra-Cebrian C, Panazzo C, Frugier T, Millet G, Robolt N, Joshi V, Melki J. Neurofilament accumulation at the motor endplate and lack of axonal sprouting in a spinal muscular atrophy mouse model. Hum Mol Genet. 2002; 11(12):1439–1447. [PubMed: 12023986]

Crawford TO, Pardo CA. The neurobiology of childhood spinal muscular atrophy. Neurobiol Dis. 1996; 3(2):97–110. [PubMed: 9173917]

Cuddon PA. Electrophysiology in neuromuscular disease. Vet Clin North Am Small Anim Pract. 2002; 32(1):31–62. [PubMed: 11785734]

Dashiell SM, Tanner SL, Pant HC, Quarles RH. Myelin-associated glycoprotein modulates expression and phosphorylation of neuronal cytoskeletal elements and their associated kinases. J of Neurochem. 2002; 81(6):1263–1272. [PubMed: 12068074]

De Lahunta, A. Neurological Examination.. In: Braun, KG., editor. Clinical Neurology in Small Animals – Localization, Diagnosis and Treatment. International Veterinary Information Service; Ithaca: 2001. p. 2-9.

Emery AE. The nosology of the spinal muscular atrophies. J Med Genet. 1971; 4:481–495. [PubMed: 4948374]

Ferri A, Melki J, Kato AC. Progressive and selective degeneration of motoneurons in a mouse model of SMA. Neuroreport. 2004; 15(2):275–280. [PubMed: 15076752]

Fyfe JC, Menotti-Raymond M, David VA, Brichta L, Schäffer AA, Agarwala R, Murphy WJ, Gregory BL, Buzzell BG, Drummond MC, Wirth B, O'Brien SJ. An ~ 140-kb deletion associated with feline spinal muscular atrophy implies an essential LIX1 function for motor neuron survival. Genome Res. 2006; 16:1084–1090. [PubMed: 16899656]

Garcia ML, Lobsiger CS, Shah SB, Deerinck TJ, Crum J, Young D, Ward CM, Crawford TO, Gotow TJ, Uchiyama Y, Ellisman MH, Calcutt NA, Cleveland DW. NF-M is an essential target for the myelin-directed “outside-in” signaling cascade that mediates radial axonal growth. J Cell Biol. 2003; 163(5):1011–1020. [PubMed: 14662745]

Garcia ML, Rao MV, Fujimoto J, Garcia VB, Shah SB, Crum J, Gotow T, Uchiyama Y, Ellisman M, Calcutt NA, Cleveland DW. Phosphorylation of highly conserved neurofilament medium KSP repeats is not required for myelin-dependent radial axonal growth. J Neurosci. 2009; 29(5):1277–1284. [PubMed: 19193875]

Ghatak NR. Spinal roots in Werdnig-Hoffmann disease. Acta Neuropathol. 1978; 41:1–7. [PubMed: 636832]

Giot L, Bader JS, Brouwer C, Chaudhuri A, Kuang B, Li Y, Hao YL, Ooi CE, Godwin B, Vitols E, Vijayadamodar G, Pochart P, Machineni H, Welsh M, Kong Y, Zerhusen B, Malcolm R, Varone Z, Collis A, Minto M, Burgess S, McDaniel L, Stimpson E, Spriggs F, Williams J, Neurath K, Ioime N, Agee M, Voss E, Furtak K, Renzulli R, Aanensen N, Carrolla S, Bickelhaupt E, Lazovatsky Y, DaSilva A, Zhong J, Stanyon CA, Finley RL Jr, White KP, Braverman M, Jarvie T, Gold S, Leach M, Knight J, Shimkets RA, McKenna MP, Chant J, Rothberg JM. A protein interaction map of Drosophila melanogaster. Science. 2003; 302(5651):1727–1736. [PubMed: 14605208]

Haynes RL, Borenstein NS, Desilva TM, Folkerth RD, Liu LG, Volpe JJ, Kinney HC. Axonal development in the cereberal white matter of the human fetus and infant. J Comp Neurol. 2005; 484:156–157. [PubMed: 15736232]

He Q, Lowrie C, Shelton GD, Castellani RJ, Menotti-Raymond M, Murphy W, O'Brien SJ, Swanson WF, Fyfe JC. Inherited motor neuron disease in domestic cats: a model of spinal muscular atrophy. Pediatr Res. 2005; 57(3):324–330. [PubMed: 15635053]

Hoffman PN, Cleveland DW, Griffin JW, Landes PW, Cowan NJ, Price DL. Neurofilament gene expression: a major determinant of axonal caliber. Proc Natl Acad Sci. 1987; 84:3472–3476. [PubMed: 3472217]

Hoffman PN, Thompson GW, Griffin JW, Price DL. Changes in neurofilament transport coincide temporally with alterations in the caliber of axons in regenerating motor fibers. J Cell Biol. 1985; 101(4):1332–1340. [PubMed: 2413041]

Hsieh ST, Kidd GJ, Crawford TO, Xu Z, Lin WM, Trapp BD, Cleveland DW, Griffin JW. Regional modulation of neurofilament organization by myelination in normal axons. J Neurosci. 1994; 14(11):6392–6401. [PubMed: 7965044]

Hausmanowa-Petrusewicz I, Fidzianska A. Spinal muscular atrophy: foetal-like histopathological pattern in Werdig-Hoffman disease. Bull N Y Acad Med. 1974; 50:1157–1172. [PubMed: 4529631]

Keller SR, Davis AC, Clairmont KB. Mice deficient in the insulin-regulated membrane aminopeptidase show substantial decreases in glucose transporter GLUT4 levels but maintain normal glucose homeostasis. J Biol Chem. 2002; 277(20):17677–17686. [PubMed: 11884418]

Kugelberg E, Welander L. Heredofamilial juvenile muscular atrophy simulating muscular dystrophy. AMA Arch Neurol Psych. 1956; 75:500–509.

Kuru S, Sakai M, Konagaya M, Yoshida M, Hashizume Y, Saito K. An autopsy case of spinal muscular atrophy type III (Kugelberg-Welander disease). Neuropathology. 2009; 29:63–67. [PubMed: 18410269]

Lee MK, Cleveland DW. Neuronal intermediate filaments. Annu Rev Neurosci. 1996; 19:187–217. [PubMed: 8833441]

Lefebvre S, Bürglen L, Reboullet S, Clermont O, Burlet P, Viollet L, Benichou B, Cruaud C, Millasseau P, Zeviani M, Le Paslier D, Frézal J, Cohen D, Weissenbach J, Munnich A, Melki J. Identification and characterization of a spinal muscular atrophy-determining gene. Cell. 1995; 80(1):155–165. [PubMed: 7813012]

Lippa C, Smith T. Chromatolytic neurons in Werdnig-Hoffmann disease contain phosphorylated neurofilaments. Acta Neuropathol. 1988; 77:91–94. [PubMed: 3149123]

Lorson CL, Androphy EJ. An exonic enhancer is required for inclusion of an essential exon in the SMA-determining gene SMN. Hum Mol Genet. 2000; 9(2):259–265. [PubMed: 10607836]

Lorson CL, Hahnen E, Androphy EJ, Wirth B. A single nucleotide in the SMN gene regulates splicing and is responsible for spinal muscular atrophy. Proc Natl Acad Sci USA. 1999; 96(11):6307–6311. [PubMed: 10339583]

Massenet S, Pellizzoni L, Paushkin S, Mattaj IW, Dreyfuss G. The SMN complex is associated with snRNPs throughout their cytoplasmic assembly pathway. Mol Cell Biol. 2002; 22(18):6533–6541. [PubMed: 12192051]

Michaud M, Arnoux T, Bielli S, Durand D, Rotrou Y, Jablonka S, Robert F, Giraudon-Paoli M, Riessland M, Mattei MG, Andriambeloson E, Wirth B, Sendtner M, Gallego J, Pruss RM, Bordet T. Neuromuscular defects and breathing disorders in a new mouse model of spinal muscular atrophy. Neurobiol Dis. 2010; 38(1):125–135. [PubMed: 20085811]

Moeller C, Yaylaoglu MB, Alvarez-Bolado G, Thaller C, Eichele G. Murine Lix1, a novel marker for subtantia nigra, corical layer 5, and hindbrain structures. Brain Res Gene Expr Patterns. 2002; 1(3-4):199–203. [PubMed: 12638132]

Monani UR, Lorson CL, Parsons DW, Prior TW, Androphy EJ, Burghes AH, McPherson JD. A single nucleotide difference that alters splicing patterns distinguishes the SMA gene SMN1 from the copy gene SMN2. Hum Mol Genet. 1999; 8(7):1177–1183. [PubMed: 10369862]

Monani UR, Pastore MT, Gavrilina TO, Jablonka S, Le TT, Andreassi C, DiCocco JM, Lorson C, Androphy EJ, Sendtner M, Podell M, Burghes AH. A transgene carrying an A2G missense

mutation in the SMN gene modulates phenotypic severity in mice with severe (type I) spinal muscular atrophy. Cell. 2003; 160:41–52.

Moosa A, Dubowitz V. Motor nerve conduction velocity in spinal muscular atrophy of childhood. Br Med J. 1976; 51:974–977.

Munsat TL, Davies KE. International SMA consortium meeting. Neuromuscul Disord. 1992; 2:423–428. [PubMed: 1300191]

Murayama S, Bouldin T, Suzuki K. Immunocytochemical and ultrastructural studies of Werdnig-Hoffmann disease. Acta Neuropathol. 1991; 81:408–417. [PubMed: 1851364]

Murray LM, Comley LH, Thomson D, Parkinson N, Talbot K, Gillingwater TH. Selective vulnerability of motor neurons and dissociation of pre- and post-synaptic pathology at the neuromuscular junction in mouse models of spinal muscular atrophy. Hum Mol Genet. 2008; 17:949–962. [PubMed: 18065780]

Pellizzoni L, Kataoka N, Charroux B, Dreyfuss G. A novel function for SMN, the spinal muscular atrophy disease gene product, in pre-mRNA splicing. Cell. 1998; 95(5):615–624. [PubMed: 9845364]

Pellizzoni L, Yong J, Dreyfuss G. Essential role for the SMN complex in the specificity of snRNP assembly. Science. 2002; 298(5599):1775–1779. [PubMed: 12459587]

Pestronk A, Drachman DB. A new stain for quantitative measurement of sprouting at neuromuscular junctions. Muscle & Nerve. 1978; 1(1):70–74. [PubMed: 88010]

Purves, D.; Augustine, GJ.; Fitzpatrick, D.; Katz, LC.; LaMantia, AS.; McNamara, JO.; Williams, SM., editors. Neuroscience. Sinauer Associates; Sunderland: 2001.

Rao MV, Campbell J, Yuan A, Gotow T, Uchiyama Y, Nixon RA. The neurofilament middle molecular mass subunit carboxyl-terminal tail domains is essential for the radial growth and cytoskeletal architecture of axons but not for regulating neurofilament transport rate. J of Cell Biol. 2003; 163(5):1021–031. [PubMed: 14662746]

Rao MV, Garcia ML, Miyazaki Y, Gotow T, Yuan A, Mattina S, Ward CM, Calcutt NA, Uchiuama Y, Nixon RA, Cleveland DW. Gene replacement in mice reveals that the heavily phosphorylated tail of neurofilament heavy subunit does not affect ax;onal caliber or the transit of cargoes in slow axonal transport. J Cell Biol. 2002; 158(4):681–693. [PubMed: 12186852]

Rao MV, Houseweart MK, Williamson TL, Crawford TO, Folmer J, Cleveland DW. Neurofilament-dependent radial growth of motor axons and axonal organization of neurofilaments does not require the neurofilament heavy subunit (NF-H) or its phosphorylation. J Cell Biol. 1998; 143(1): 171–181. [PubMed: 9763429]

Russman BS. Spinal muscular atrophy: clinical classification and disease heterogeneity. J Child Neurol. 2007; 22(8):946–951. [PubMed: 17761648]

Sakaguchi T, Okada M, Kitamura T, Kawasaki K. Reduced diameter and conduction velocity of myelinated fibers in the sciatic nerve of a neurofilament-deficient mutant quail. Neurosci Lett. 1993; 153(1):65–68. [PubMed: 8510825]

Sato M, Mizuno N, Konishi A. Postnatal differentiation of cell body volumes of spinal motoneurons innervating slow-twitch and fast-twitch muscles. J Comp Neurol. 1977; 175(1):27–36. [PubMed: 886025]

Sternberger LA, Sternberger NH. Monoclonal antibodies distinguish phosophorylated and non-phosphorylated forms of neurofilaments in situ. Proc Nat Acad Sci USA. 1983; 80:6126–6130. [PubMed: 6577472]

Tatton WG, Theriault E. Postnatal growth of medial gastrocnemius motoneurons in the kitten. Brain Res. 1988; 471(2):191–206. [PubMed: 3179749]

Ulfig N, Nickel J, Bohl J. Monoclonal antibodies SMI 311 and SMI 312 as tools to investigate the maturation of nerve cells and axonal patterns in human fetal brain. Cell Tissue Res. 1998; 291:433–443. [PubMed: 9477300]

Walsh F, Moore S, Lake B. Cell adhesion molecule N-CAM is expressed by denervated myofibres in Werdnig-Hoffman and Kugelberg-Welander type spinal muscular atrophies. J Neurol Neurosurg Psychiatry. 1987; 50:439–442. [PubMed: 3295121]

Wirth B, Herz M, Wetter A, Moskau S, Hahnen E, Rudnik-Schöneborn S, Wienker T, Zerres K. Quantitative analysis of survival motor neuron copies: identification of subtle SMN1 mutations in

patients with spinal muscular atrophy, genotype-phenotype correlation, and implications for genetic counseling. Am J Hum Genet. 1999; 64(5):1340–1356. [PubMed: 10205265]

Wirth B, Brichta L, Hahnen E. Spinal muscular atrophy: from gene to therapy. Semin Ped Neurol. 2006; 13(2):121–131.

Yin X, Crawford TO, Griffin JW, Tu P, Lee VM, Li C, Roder J, Trapp BD. Myelin-associated glycoprotein is a myelin signal that modulates the caliber of myelinated axons. J Neurosci. 1998; 18(6):1953–1962. [PubMed: 9482781]

Zhang H, Xing L, Singer RH, Bassell GJ. QNQKE targeting motif for the SMN-Gemin multiprotein complex in neurons. J Neurosci Res. 2007; 85(12):2657–2667. [PubMed: 17455327]

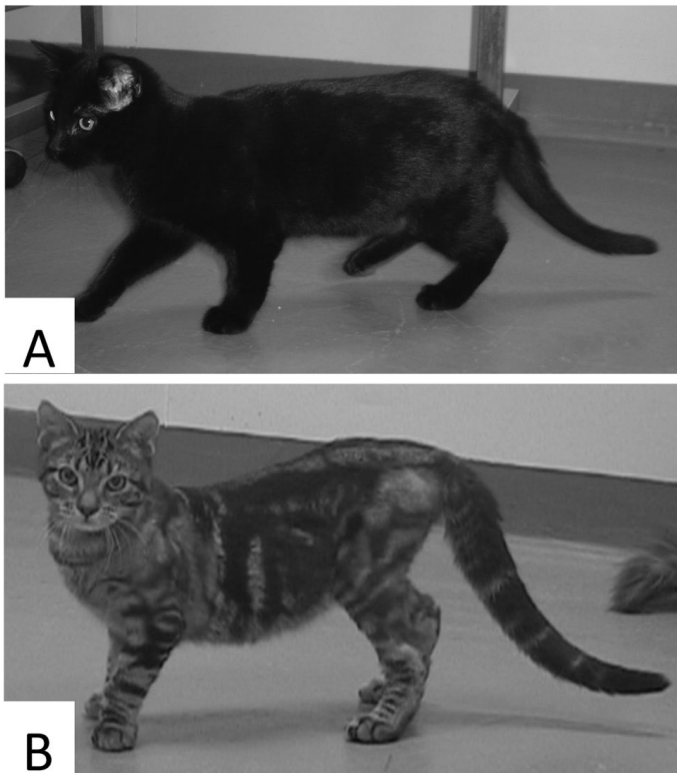

Figure 1.
Photographs of a normal (A) and an affected cat (B) aged 20 weeks. Typical feline SMA signs include curvature of the spine, lateral deviation of the front paws, increased width of the hind-limb support polygon, hind-limb muscle atrophy and touching of the tarsal joints.

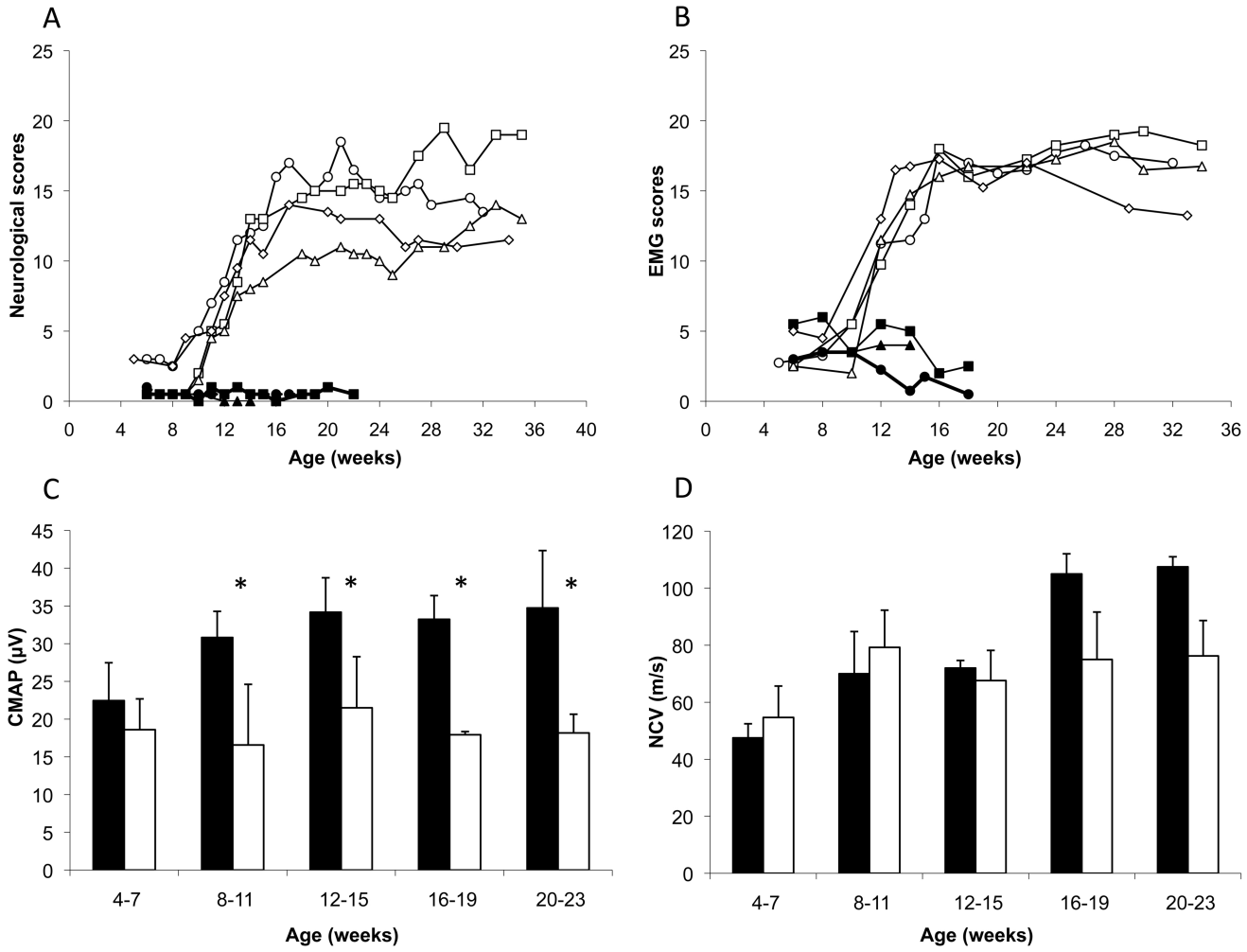

Figure 2.

Evolution of (A) neurological signs and (B) electromyographic (EMG) abnormalities, scored according to severity, in 3 normal cats (solid symbols) and 4 affected (open symbols) from 4 to 36 weeks of age. (C) Compound muscle action potentials (CMAP) measured in soleus muscle after a stimulation of the sciatic nerve. (asterisks indicate statistical significance at $p<0.05$), and (D) nerve conduction velocities (NCV) of the sciatic nerve in normal (solid bars) and affected (open bars) cats.

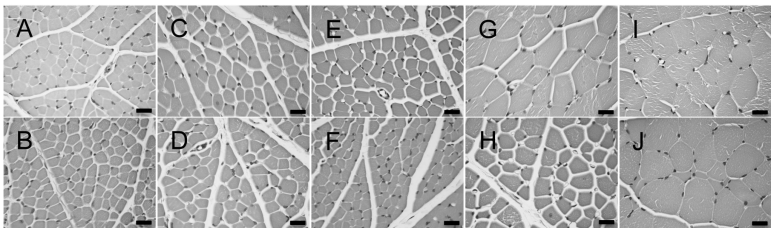

Figure 3.

Photomicrographs of H&E stained cross sections of quadriceps muscle. B, D, F, H and J are representative images from affected cats. A, C, E, G and I are from age matched controls. Cats were aged 6 wks (A, B), 8 wks (C, D), 10 wks (E, F), 12 wks (G, H) or 21 wks (I, J) when euthanized. Bars = 20 μm.

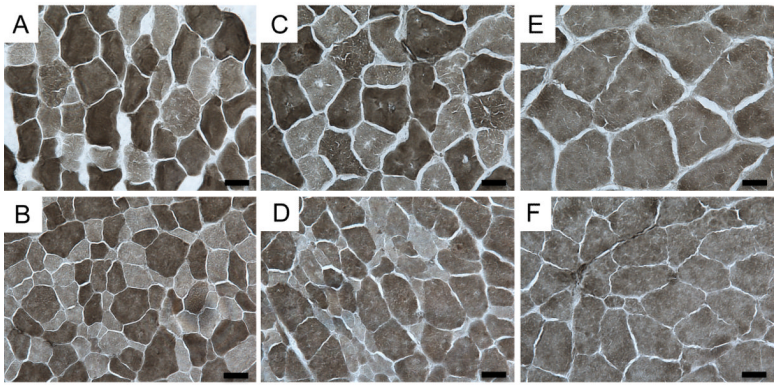

Figure 4.

Photomicrographs of fiber-typed hind limb muscles. TA (A, B), EDL (C, D) and soleus (E, F) from 12 week old SMA affected (B,D F) and control (A,B,C) cats were fiber typed by myofibrillar ATPase reaction at pH 4.6. At this pH, type I (slow twitch) fibers are lightly stained. Both type I and type II (fast twitch) atrophic fibers were observed in affected cats, although the majority of atrophic fibers were Type II. Bars = 20 μm.

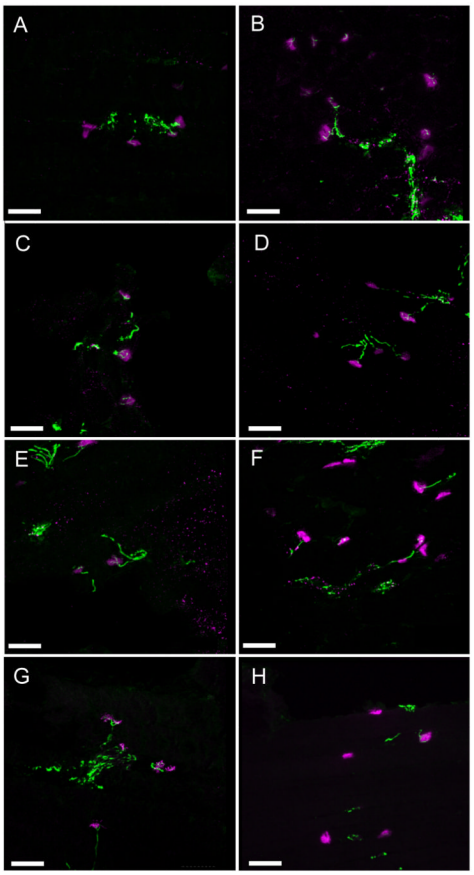

Figure 5.

Extended focus images of TA and EDL neuromuscular junctions by confocal laser scanning microscopy. Acetylcholine receptors are labeled in magenta and neurofilaments are labeled in green. B,D,F and H are representative images from SMA affected TA (B and F) and EDL (D and H) sections at 10 (B and D) and 12 weeks (F and H). A,C,E and G are representative images from age and tissue matched controls. A) 35 optical sections representing a thickness of 10.5 μm. B) 60 optical sections representing a thickness of 18 μm. C) 71 optical sections representing a thickness of 14.2 μm. D) 61 optical sections representing a thickness of 18.3 μm. E) 68 optical sections representing a thickness of 20 μm. F) 65 optical sections representing a thickness of 19.5 μm. G) 76 optical sections representing a thickness of 15.2 μm. H) 91 optical sections representing a thickness of 18.2 μm. Bar = 50 μm.

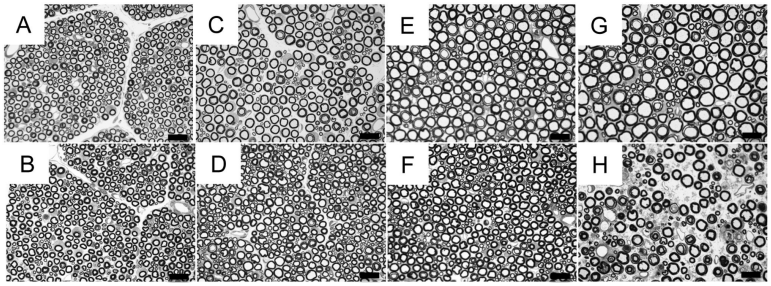

Figure 6.

L5 toulidine blue stained ventral roots. Panels A-H are representative images of normal (A, C, E, and G) and affected cat (B, D, F, and H) ventral roots at 4.5 weeks (A and B), 8-9 weeks (C and D), 12 weeks (E and F) and 21 weeks (G and H). Bar = 20 μm.

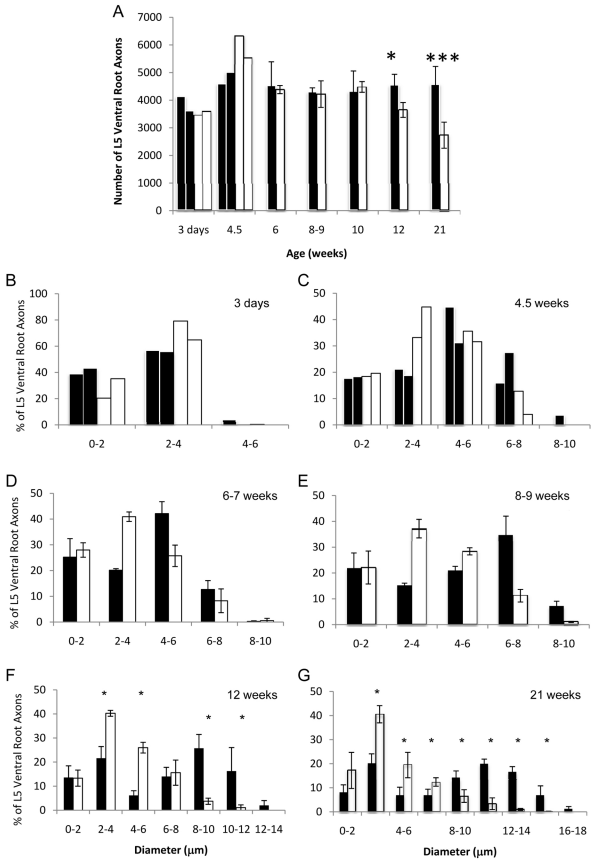

Figure 7.

L5 motor neuron axons counts and morphometrics. A) Total number of myelinated axons in L5 ventral root in normal (shaded) and affected (un-shaded) cats. A single asterisk denotes statistical significance by Student's t-test ($p<0.03$, n=3 except at 21 weeks, where n=5). Three asterisks denote statistical significance by Student's t-test ($p<0.001$). L5 ventral roots axon morphometrics at 3 days (B), 4.5 weeks (C), 6 weeks (D), 8-9 weeks (E) 12 weeks, (F), and 21 weeks, (G), of normal (shaded) and affected cats (un-shaded). In B, and D, n=2. At all other time points, n was greater than or equal to 3, and thus averages ± S.D. were graphed. A single asterisk denotes statistical significance by Mann Whitney U test ($p<0.03$, n=4 at 12 weeks and at 21 weeks, where n=5).

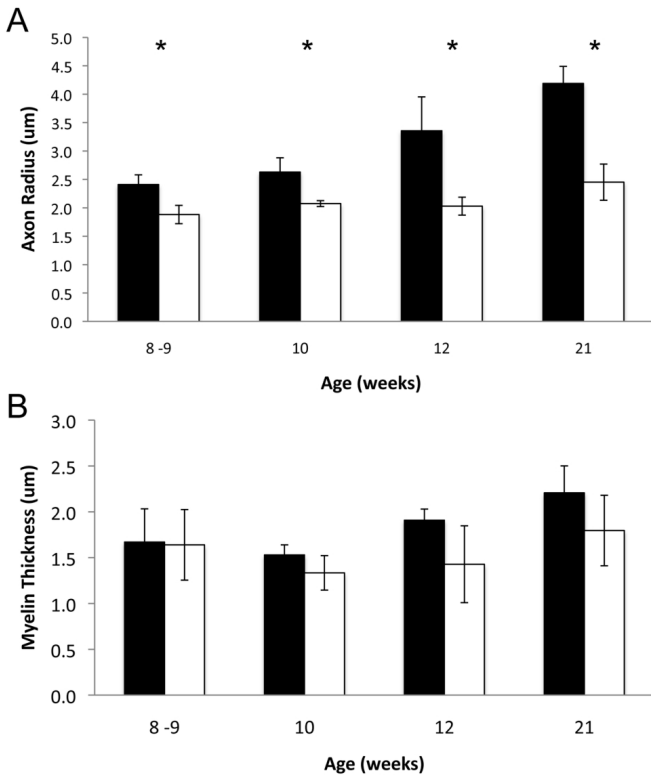

Figure 8.

Average axon radius and myelin thickness. A) Average L5 ventral root axon radius as measured in 100 axons from normal (shaded) and affected (un-shaded) cats. B) Average myelin sheath thickness measured in the same 100 axons (n=3 except at 21 weeks where n=5). Asterisks indicate statistical significance by Student's t-test ($p \leq 0.02$).

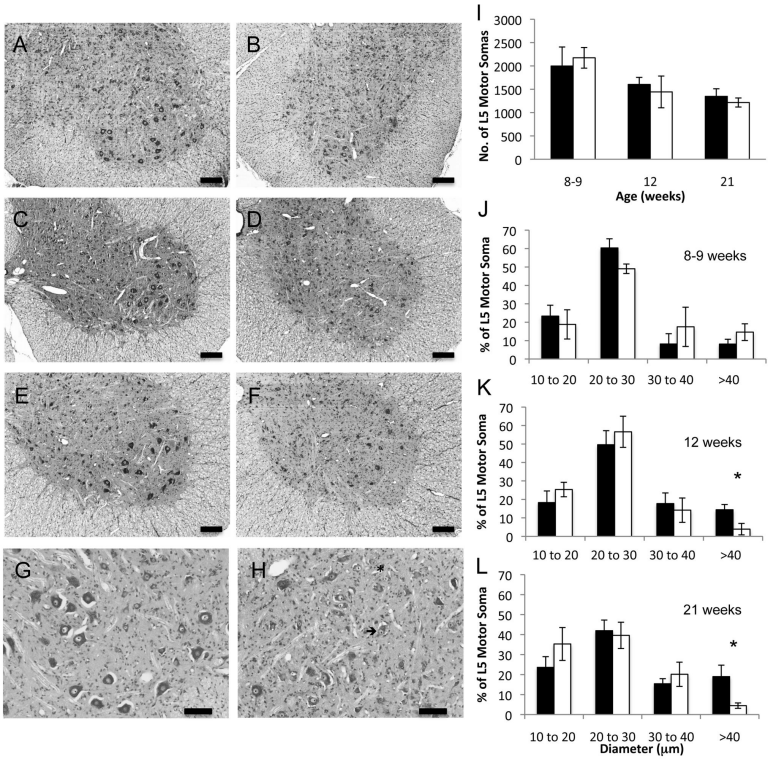

Figure 9.

Cresyl violet stained L5 spinal cord and soma counts and morphometrics. Photomicrographs of L5 anterior horns from normal cats aged 8 wks (A) 12 wks (C) and 21 wks (E) and from age matched affected cats B, D, and F, respectively. Bars=200 μm. G (normal cat, 8 weeks) and H (affected cat, 8 weeks) photomicrographs were taken at a higher magnification (bar = 100 mm) to demonstrate the presence of chromalytic cells (asterisk) and acentric nuclei (arrow) in affected cats. I) Number of motor neuron somas counted in 160 mm of cresyl violet stained L5 spinal cord. Average ± S.D shown. Cell body morphometrics at 8-9 wks (J), 12 wks (K) and 21 wks (L). Averages ± S.D. for normal (shaded) and affected cats (un-shaded) are shown. Asterisks indicate statistical significance by Mann-Whitney U test with $p \leq 0.03$.

Table 1

Primary Antibody

Antigen	Immunogen	Manufacturer, species, type, cat. no.	Dilution
Phosphorylated heavy and medium neurofilament proteins [SMI-312]	Homogenized Fisher 344 rat hypothalamus	Abcam (Cambridge, MA), mouse monoclonal cocktail, no. ab24574, lot 616423	1:1,000

Table 2

Summary of muscle fiber size and L5 axon and cell body counts. Statistical significance at $p<0.05$ is denoted by a single asterisk.

	Quadricep Muscle Fiber Diameter (μm)		L5 Motor Axon Number		L5 Motor Soma Number	
Age	**Normal**	**Affected**	**Normal**	**Affected**	**Normal**	**Affected**
3 days	--	--	4130 3612	3594 3456	--	--
4.5 weeks	--	--	5023 4598	5544 6342	--	--
6 weeks	16.0±2.6 12.0±2.5	16.6±4.2 14.4±2.8	4524±867 (n=3)	4385±147 (n=3)	--	--
8-9 weeks	18.2±4.6 18.8±3.6	18.2±3.6 16.6±4.2	4297±151 (n=3)	4221±481 (n=3)	1456±277 (n=3)	1539±143 (n=3)
10 weeks	17.2±3.8 22.9±4.3	14.5±2.6 11.6±1.9	4312±747 (n=3)	4481±194 (n=3)	--	--
12 weeks	--	--	4543±396 (n=4)	3647±269* (n=4)	1187±101 (n=4)	1072±259 (n=4)
21 weeks	--	--	4575±648 (n=5)	2734±472* (n=5)	967±105 (n=5)	787±63 (n=5)